J Mol Model (2010) 16:1401–1413
DOI 10.1007/s00894-010-0644-5

ORIGINAL PAPER

Theoretical investigation of the ring opening process of verdoheme to biliverdin in the presence of dioxygen

Mahin Gheidi · Nasser Safari · Mansour Zahedi

Received: 27 October 2009 / Accepted: 10 December 2009 / Published online: 16 February 2010

Abstract The conversion of ferrous verdoheme to ferric biliverdin in the presence of O_2 was investigated using the B3LYP method. Both 6-31G and 6-31G (d) basis sets were employed for geometry optimization calculation as well as energy stabilization estimation. Three possible pathways for the conversion of iron verdoheme to iron biliverdin were considered. In the first route oxygen and reducing electron were employed. In this path formation of ferrous verdoheme-O_2 complex was followed by the addition of one electron to the ferrous-oxycomplex to produce ferric peroxide intermediate. The ferric peroxide intermediate experienced an intramolecular nucleophilic attack to the most positive position at 5-oxo carbons on the ring to form a closed ring biliverdin. Subsequently the ring opening process took place and the iron (III) biliverdin complex was formed. Closed ring iron biliverdin intermediate and open ring iron biliverdin formed as a product of verdoheme cleavage were respectively 13.20 and 32.70 kcal mol^{-1} more stable than ferric peroxide intermediate. Barrier energy for conversion of ferric peroxide to closed ring Fe (III) biliverdin and from the latter to Fe (III) biliverdin were respectively 8.67 and 3.35 kcal mol^{-1}. In this path spin ground states are doublet except for iron (III) biliverdin in which spin state is quartet. In the second path a ferrous-O_2 complex was formed and, without going to a one electron reduction process, nucleophilic attack of iron superoxide complex took place followed by the formation of iron (III) biliverdin. This path is thermodynamically and kinetically less favorable than the first one. In addition, iron hydro peroxy complex or direct attack of O_2 to macrocycle to form an isoporphyrin type intermediate have shown energy surfaces less favorable than aforementioned routes.

Keywords B3LYP · Ferric biliverdin · Ferrous verdoheme · Homolytic · O_2

M. Gheidi · N. Safari (✉) · M. Zahedi
Department of Chemistry, Faculty of Sciences,
Shahid Beheshti University,
G. C., Evin,
19839-63113 Tehran, Iran
e-mail: n-safari@cc.sbu.ac.ir

Introduction

Heme catabolism is an important physiological process that converts heme to the biliverdin in the presence of heme oxygenase [1–3]. Not only does this process have an essential role for destroying unwanted heme, but also the intermediates in this process, such as biliverdin, are found to have antioxidant roles for oxidative stress [4, 5], Scheme 1.

In the heme oxygenates degradation of heme, the mechanism that converts verdoheme into biliverdin is the least known step and is the subject of challenges. Different pathways have been proposed for the conversion of iron verdoheme to iron biliverdin. In one path, the ferrous verdoheme reacts with O_2 in a manner similar to the Cythochrome P-450 enzymes to produce ferric superoxide and further to peroxide intermediates which then decays to iron biliverdin *via* a rebound mechanism. There is another path assumed in which direct nucleophilic attack of O_2 takes place at the carbon position adjacent to the *meso*-oxygen on the ferrous verdoheme or on the reduced form of the iron verdoheme, [6–11] Scheme 2. The third conversion path (for the conversion of iron verdoheme into iron biliverdin) involves hydrolysis of iron verdoheme (the former) which has been proposed based on model studies and theoretical investigations [5, 12].

In this investigation *ab initio* DFT method has been employed to investigate the conversion of iron verdoheme to

Scheme 1 Conversion of heme to ferric-bilivverdin IXα complex

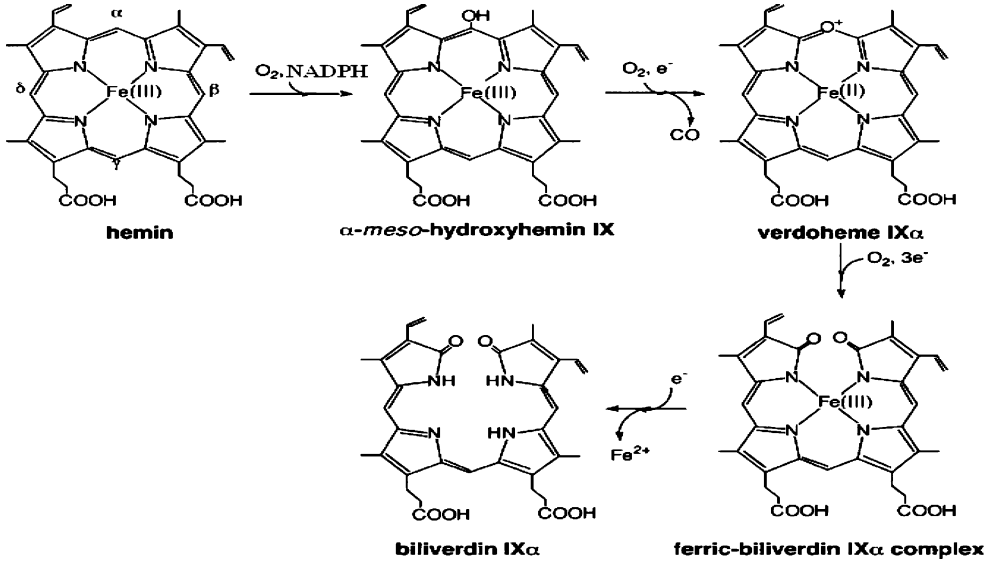

iron biliverdin, while all the side chains are eliminated and replaced by hydrogen to speed up the calculation process. In this study 6-31G and 6-31G (d) basis sets have been utilized. The details of ligation and spin states of iron have been thoroughly discussed and so has the possibility of direct attack of the dioxygen on the metal or macrocycle. Based on the results obtained in this study a mechanistic pathway for the conversion of verdoheme into biliverdin has been proposed.

Methods

Computational methods

All calculations were performed with a legally licensed version of the Gaussian 98 program [13] using facilities at the institute of postgraduate studies, University of Malaya, Kuala Lumpur, Malaysia. The energies and geometries of

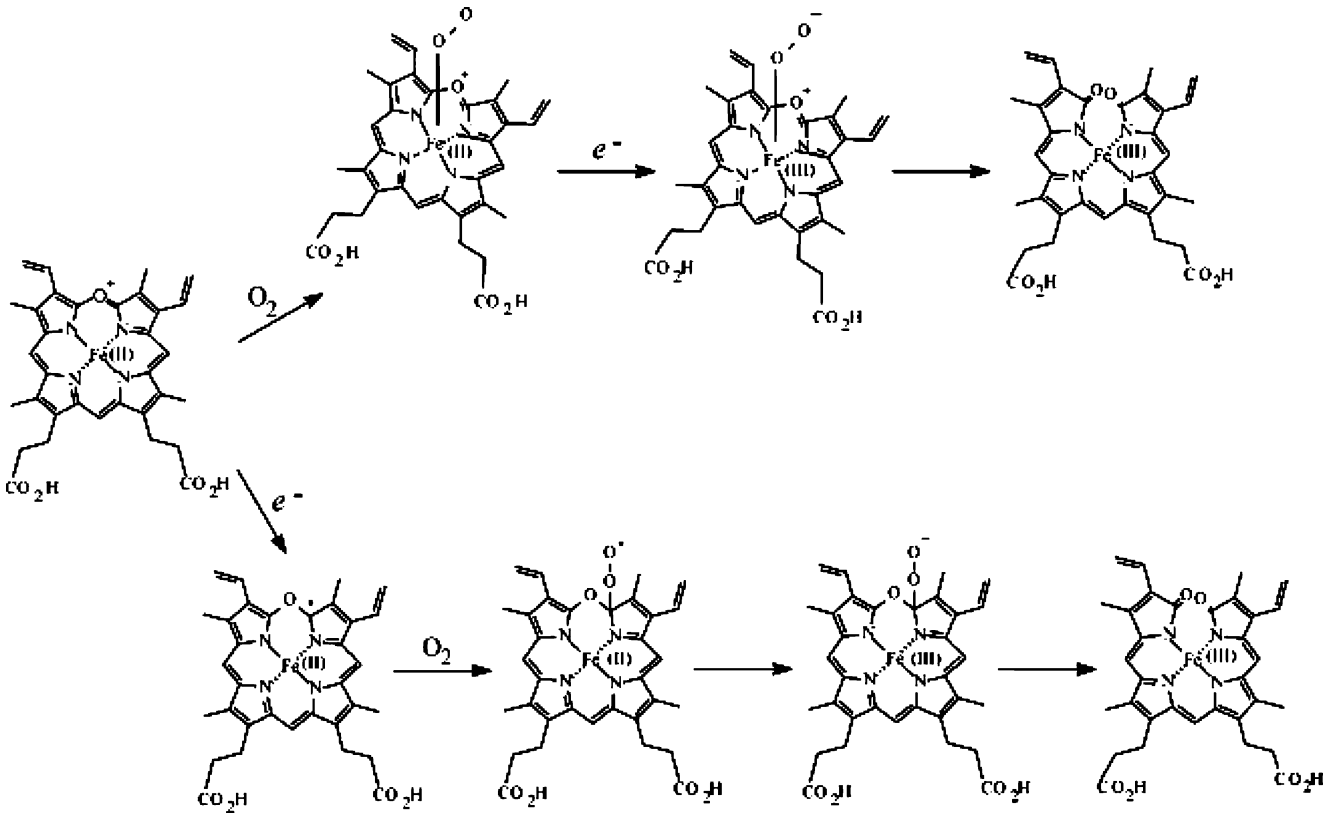

Scheme 2 Pathways for the conversion of iron verdoheme to iron biliverdin

different complexes were calculated and optimized with the Lee Yang, and Parr (LYP) [14] functional, denoted B3LYP [15] of which the most successful one is based on the hybrid functional method [16]. We have used B3LYP [17] method and 6-31G, 6-31G (d) [18, 19] basis functions in this investigation, B3LYP/6-31G method is used for optimization of all structures and B3LYP/6-31G (d) method is employed for energy calculation of these optimized structures. The spin unrestricted version of B3LYP (UB3LYP) method was applied even to singlet states when the reaction species are reasonably considered to have an open-shell-singlet electronic configuration [20–24].

Compounds **3** and **5** in the doublet states have significant spin contamination which leads to the possibility of contribution to an admixture of high spin states. To account for spin contamination, a correction based on the expectation value of S^2 calculated over de kohn-sham determinants is used even though these determinants are not eigenvalues of the S^2 operator. Subtraction of the energy contribution of the higher spin states, Es+1, from the spin contaminated energy, EC, and renormalization yields an estimate of the energy of the desired pure spin state, Es [25, 26],

$$a = \frac{\langle S^2 \rangle_C - s(s+1)}{2(s+1)} \quad (1)$$

$$E_S = \frac{E_C - aE_{s+1}}{1-a} \quad (2)$$

Assuming that in the spin-crossover complex the B3LYP method may not accurately predict spin states energies, particularly when energy difference is less than 10 kJ mol^{-1}. Thus B3LYP* as well as B3LYP is benefited for compounds **3**, **4**, and **5** which have close spin energy states. A modification of B3LYP to B3LYP* [27–29], where the Hartree-Fock exchange was reduced by 5% (from 20% to 15%) is also used. the spin state energies and geometries of compounds **3**, **4**, and **5** were calculated with this new functional.

Full optimizations of the studied compounds in different spin states, without any symmetry constraint, have been performed with FOPT keyword. The optimized structures for all species are presented in supplementary materials. Harmonic vibrational frequencies were systematically computed to confirm whether an optimized geometry correctly corresponds to a local minimum that has only real frequencies or to a transition state which has just one imaginary frequency. Atomic charge and spin density studies were based on Mulliken calculation. The natural bond orbital (NBO) analysis has been used to explain α and β spin distribution in d orbitals of iron and the macrocycle ring as well as to assign the atomic charges.

Model used and choice of initial geometries

The model of the verdoheme site used in all DFT calculations is an iron verdoheme complex taken from the crystal structure of iron complexes of octaethyloxoporphyrin [30] after substituting the ethyl group with hydrogen and replacing the axial ligands with an imidazole. The structure is optimized by DFT methods. The O_2 is closed from opposite sites of imidazole in different orientations. In all cases the coordinated O_2 is optimized in the orientations shown in traces of **a**–**d** in Fig. 1. The **a**–**d** orientations have similar energy within 1 kcal mol^{-1}. The configuration **a**, in Fig. 1 is chosen as the initial configuration for species shown in energy surface in Fig. 3. With this initial configuration, barrier energy toward the final product is minimized and this system was subjected to energy optimization. Thus the optimized structure of compound **3** was then used to construct the initial model of the intermediate **4**.

Results

Conversion of iron (II) verdoheme, 1 to iron (III) biliverdin, 5 in the presence of O_2 and an electron

Atom numbering presented in Fig. 2 and compound numbering, in Scheme 3 have been preserved in this study. Energies and geometries of compound **1**, **2**, and **2a** were computed and optimized in singlet; triplet and quintet spin state. Calculated Mulliken charges show that positive charges on the carbons adjacent to the 5-oxo and iron center are 0.57 and 1.68 respectively. There is a possibility for the nucleophile, to attack the iron atom first (ferrous verdoheme-O_2, **2**). Iron can then transfer the oxygen atom to the most positive part of the macrocycle, which are C8 or C9 attached to the 5-oxo position. The other possibility is the direct attack of O_2 on the C8 or C9 of the macrocycle (compound **2a**). Then the carbon can transfer the oxygen atom to the iron center. In compound **2** the triplet state is 20 kcal mol^{-1} more stable than the compound **2a**. Table 1, shows calculated relative stabilization energies for compounds **1**, **2** and **2a**. All the reported energies are relative to the zero energy of compound **2** in the triplet spin state and compound **3** in the doublet spin state.

Addition of one electron to the ferrous-oxy complex, **2**, forms a ferric peroxide intermediate, **3**. In compound **3** the doublet state is 4.45 kcal mol^{-1} more stable than the quartet state. Nucleophilic attack of O_2 to the most electrophilic carbon, 5-oxo-carbons, on the macrocycle does not change spin states of the iron in the closed ring of **4** and still the doublet state is 10.5 kcal mol^{-1} more stable than the quartet. However, when the ring is opened and an obtained

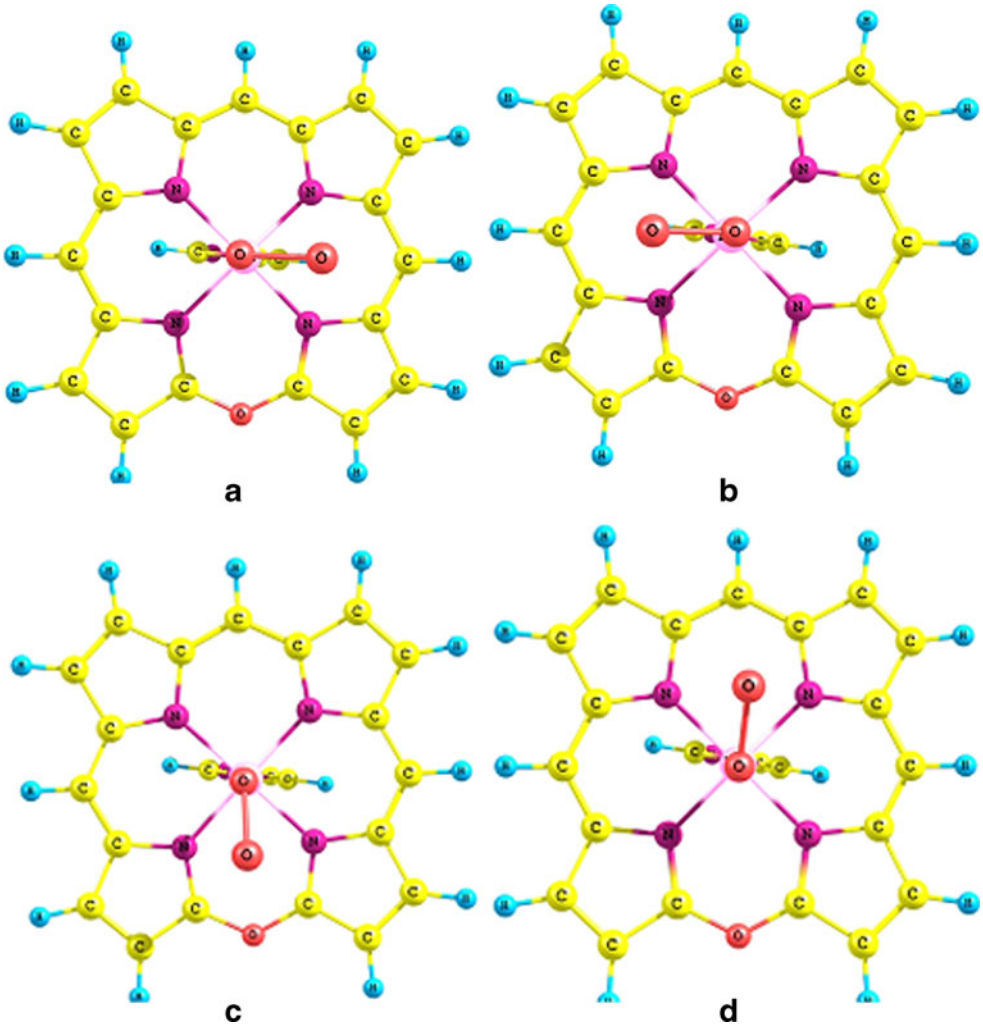

Fig. 1 Optimized structures for different orientations of O_2, Trace a is selected as initial configuration

open chain structure is fully optimized, the iron biliverdin, **5**, is more stable in the quartet state compared to that of the doublet state by about 3.34 kcal mol^{-1} (Scheme 3). Table 2, shows calculated relative energy stabilization for compounds **3–5** and involved transition states.

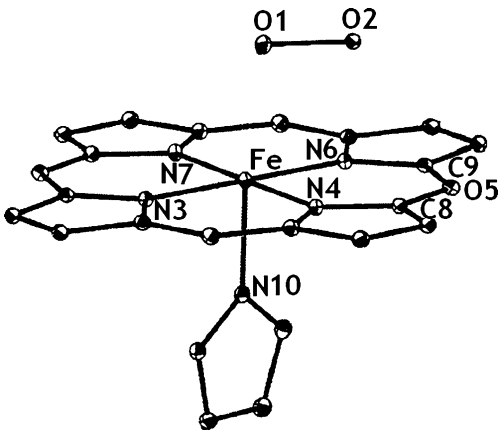

Fig. 2 Atom numbering for imidazole verdoheme and O_2 nucleophile

The details of bond distances for compounds **1–7** are given in Table 3 and the optimized structures are presented in the supplementary material.

Conversion of iron (II) verdoheme, 2, to iron (III) biliverdin, 7, in the presence of O_2

The reaction pathway for the conversion of iron verdoheme to iron biliverdin with O_2 was followed once again while oxygenated ferrous verdoheme, the [(Im) Fe (OP) (O_2)] $^+$, **2**, functions as a reactant before any reduction process (Scheme 3). In this case the nucleophilic attack can occur to the iron and 5-oxo carbon on the macrocycle. The details of stabilization energies in triplet states of iron have been presented for compounds **2**, **6**, and **7** as well as for transition states in Table 4. This table indicates that other possible spin states have higher energy than triplet state.

In complex **2**, intramolecular nucleophilic reaction of axial O_2 to *oxo* carbon, in the absence of any reducing agent, produces closed ring iron biliverdin, **6**, followed by the

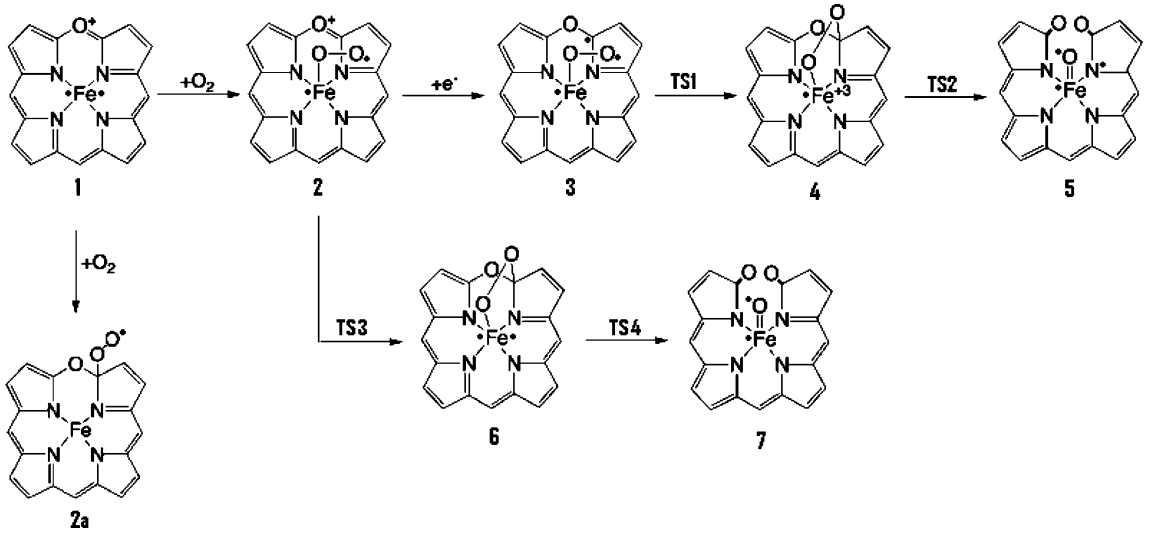

Scheme 3 Conversion of iron (II) verdoheme **1**, to iron (III) biliverdin **5**, in the presence of O_2 and an electron

formation of iron (III) biliverdin, **7**. Optimized structures are presented in supplementary material.

Protonation of ferric peroxide intermediate, **3**

Conversion process of iron verdoheme to iron biliverdin was theoretically investigated in the presence of H^+. Two oxygen atoms in intermediate **3** have a tendency to react with H^+ and their reaction is exothermic. However the protonation of terminal oxygen in **8** bears 28 kcal mol^{-1} more stabilization energy than coordinated oxygen. On the other hand protonation of terminal oxygen results in biliverdin formation, but protonation of coordinated oxygen makes the hydroxyl iron verdoheme complex. Therefore protonation on the terminal oxygen was further studied. The details of bond distances and the optimized structures for compounds **8–10** are presented in the supplementary material.

Discussion

A number of scientists have illustrated that density functional theoretical methods are strong tools in characterizing enzymatic cycles in living organisms, even when these pathways involve putative transient intermediates that have not been observed experimentally [31–39]. Considerable amount of works have been performed to clarify Cytochrom P-450 catalytic cycle [23, 40, 41]. In regard to the heme cleavage system and in spite of a large body of experimental research in recent years little attention has been paid to the theoretical study of this important biological process [42–44].

Due to the resemblance of heme-HO complex to myoglobin some authors have assumed that the ferric heme iron in the heme-HO complex at neutral pH is six-coordinate, whereas some others based on the X-ray and spectroscopic data concluded that heme-HO complex is coordinated by a proximal histidin residue and by a distal H_2O or OH^- ligand [45–50]. However, the similarity of myoglobin with heme-HO complex is in accord with iron (II) oxidation state. Based on the presented data, in the following, three pathways for

Table 1 Calculated relative energies for compound **1, 2** and **2a** using B3LYP/6-31G* method

Compounds	Energy stabilization (kcal.mol^{-1})		
	Singlet	Triplet	Quintet
1	45.83 [a]	32.63 [a]	35.93 [a]
2	14.55	0.00	16.70
2a	28.20	20.06	17.50
7	−3.00	−21.18	−7.20

[a] relative energy of **1** plus an O_2

Table 2 Calculated relative energies for conversion 3 to 5 pathway using B3LYP/6-31G* and B3LYP*/6-31G* (in parenthesis) methods

Compounds	Energy stabilization (kcal.mol^{-1})	
	Doublet	Quartet
3	0.00	4.45
	(0.00)	(9.41)
TS1	8.67	19.70
	——	——
4	−13.24	−1.50
	(−8.50)	(7.20)
TS2	−9.85	3.26
	——	——
5	−29.36	−32.70
	(−34.26)	(−35.89)

Table 3 Calculated selected bond distances for species produced using B3LYP/6-31G method

Structure	Compound 2. Triplet	Compound 3. Doublet	TS1 Doublet	Compound 4. Doublet	TS2 Doublet	Compound 5. Quartet	TS3 Triplet	Compound 6. Triplet	TS4 Triplet	Compound 7. Triplet
O1-O2	1.40	1.39	1.40	1.59	1.86	2.96	1.41	1.55	2.11	2.97
Fe-O1	1.85	1.80	1.80	1.76	1.65	1.64	1.85	1.77	1.63	1.64
Fe-N10	2.00	2.01	1.98	2.01	2.09	2.13	1.97	2.00	2.10	2.10
O2-C8	3.74	3.77	1.93	1.43	1.36	1.22	1.90	1.43	1.28	1.22
C8-O5	1.35	1.36	1.39	1.48	1.52	2.81	1.38	1.48	1.75	2.84
Fe-N3	1.96	1.97	1.97	1.95	1.95	1.97	1.96	1.93	1.95	1.95
Fe-N4	1.97	1.98	1.91	1.87	1.86	1.90	1.90	1.81	1.87	1.90
Fe-N6	1.97	1.98	1.97	1.96	1.96	1.93	1.96	1.94	1.95	1.92
Fe-N7	1.98	1.97	1.95	1.96	1.96	1.97	1.96	1.95	1.95	1.95

computational studies on the conversion of verdoheme to biliverdin have been employed. Computed stabilization energies and optimized geometries for the reaction pathways are summarized in Figs. 2 and 3.

Energy surfaces for conversion of 3 to 5

Let's take a look at the energy surfaces along the reaction pathway. Figure 3 demonstrates the computed energy surfaces and optimized geometries of verdoheme in the presence of dioxygen and an electron. The doublet and quartet potential energy surfaces are close in the entire reaction pathway: For example, the structures were optimized for O_2 attached to the iron in compound, **3**, and energy calculations employing B3LYP. Results show that for these species doublet state (ground state) is 4.45 kcal mol^{-1} more stable than the quartet state. Optimization of compound **3** while applying B3LYP* method reveals that doublet state is 9.41 kcal mol^{-1} more stable than quartet (Table 2). Transition states were found for the conversion of **3** to **4** in the doublet and quartet states for the O1-O_2 bond dissociation. As the energy surfaces in Fig. 3 shows, O_2 can transfer by a concerted rebound mechanism from the iron to carbons attached to the 5-oxo position of the macrocycle. The activation barrier for formation of intermediate **4** in this reaction is around 8.67 and 15.25 kcal mol^{-1} for the doublet and quartet state respectively. Details of energy calculations show that, the conversion process of compound **3** (doublet state) results in an intermediate **4**, which is 13.24 kcal mol^{-1} more stable than compound **3** (8.50 kcal mol^{-1} by B3LYP*). Thus, the ground states of compounds **3** and **4** are doublet. However, the open chain biliverdin in **5** was more stable in the quartet state by 3.34 kcal mol^{-1}. Using B3LYP* the energy difference is 1.63. To interest the trend of the spin states energies are similar in B3LYP and B3LYP*, although the relative energies changes are around 1.63-4.96 kcal mol^{-1}. The energy surfaces in Fig. 3 also suggest that spin inversion most likely took place during the course of reaction after TS2. However the difference between stabilization energies of doublet and quartet states for **5** is just 3.34 kcal mol^{-1} in the gas phase. In the protein environment or in the solution there is a possibility for either the stabilization of doublet or the presence of both spin states.

The barrier of TS2 relative to the intermediate **4** is 3.35 kcal mol^{-1} on the doublet energy surface and 4.76 kcal mol^{-1} on the quartet energy surface. The ring opening process from compound **4** (doublet state) to **5** (quartet state) is exothermic with $\Delta E = 10$ kcal mol^{-1} which results in an instantaneous ring opening. The optimized structures for **TS1** and **TS2** in the doublet potential curve have imaginary frequency modes at 415 and 209 cm^{-1}, respectively.

This energy surfaces shows that verdoheme is very vulnerable to the presence of O_2. Therefore Fig. 3 indicates that from a thermodynamic and kinetic point of view, iron verdoheme, **3**, is converted to **5** rapidly under aerobic condition. However in this reaction profile, rate determining step is the homolysis cleavage of oxygen-oxygen bond and transfer of the terminal oxygen from ferric peroxide complex to the macrocycle ring. In the first step of the heme degradation formation of oxy-*meso* porphyrin by concerted mechanism has a high kinetic barrier and hydrogen bonding from water network or stepwise addition of oxygen is proposed [23].

Table 4 Calculated relative energies for conversion **2** to **7** pathway using B3LYP/6-31G* method

Compounds	Energy stabilization (kcal.mol^{-1})
2	0.00
TS3	7.20
6	−2.00
TS4	3.20
7	−21.18

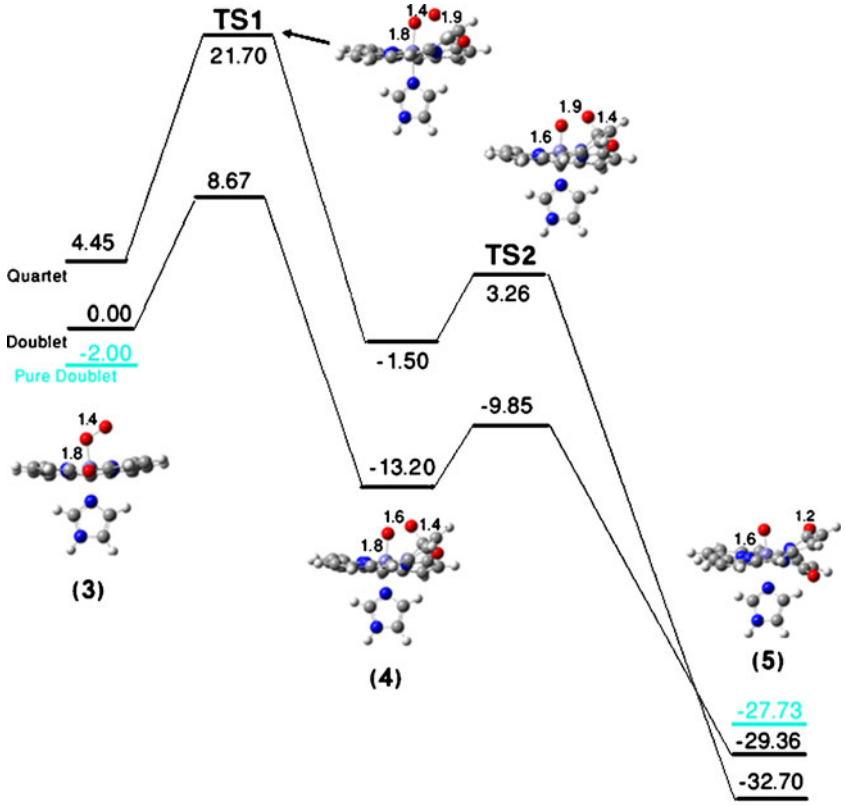

Fig. 3 Computed energy diagram with optimized structures for the reaction species of conversion 3 to 5. Energy in unit of kcal mol^{-1} and bond distances in unit of Å

Energy surfaces for conversion of 2 to 7

Computational data for electronic and spin state of the species in this pathway are presented in Table 5 and electronic structure of iron (II) verdoheme **1** and **2** are shown in Scheme 3 [12].

[(Im) Fe (OP)] $^{+}$, **1**, in the triplet state is 3.3 kcal mol^{-1} more stable than quintet and the unpaired electrons are localized on the iron atom (spin density 1.97). The ground state of [(Im) Fe (OP) (O_2)] $^{+}$, **2**, are also triplet. However, as it is shown in Scheme 3, one of the unpaired electrons is shifted to the O_2 in compound **2** (spin density on the iron 1.03 and on the oxygen 0.74). In the Fig. 4 the triplet state was the ground state for the entire pathway, Table 1, and we did not include other spin states on the figure.

As the energy surfaces in Fig. 4 shows O_2 can transfer by a rebound mechanism from the iron to carbons attached to the 5-oxo position of the macrocycle, intermediate **6**. The activation barrier for this reaction is about 7.2 kcal mol^{-1}. Detail of energy calculations indicate that, the intermediate **6** is only 2 kcal mol^{-1} more stable than compound, **2**. Low barrier energy for converting **2** to **6** and the almost similar energy difference between them demonstrates a reversible equilibrium process for conversion of **2** to **6**.

As Fig. 3 suggests, TS1 has low barrier (8.67 kcal mol^{-1}). Such low barrier can be explained by *alpha* spin densities on the ring (0.92) and *beta* spin density on the terminal oxygen (O_2=−0.71), therefore spin pairing has occurred in relatively low energy. However, low barrier for TS3 is seen in Fig. 4, whereas there are no considerable spin densities on the oxygen and the ring. The latter low barrier of TS3 may be accounted for by charge densities of TS3 in Fig. 3 as compared to that of TS1 in Fig. 3. The charge separation in TS1 is larger than TS3 which makes it less stable (ring charge of −1.30 relative to that of −0.50).

Formation of iron biliverdin, **7**, from **2** is −21 kcal mol^{-1} exothermic, while energy stabilization for converting **3** to **5** is −32.7 kcal mol^{-1}. Therefore we assume that conversion of verdoheme to biliverdin in the presence of O_2 follows the route presented in Fig. 4. However it is not possible to exclude the route presented in Fig. 4 since its energy surfaces predicts possibility of it route. The barrier of TS4 relative to the intermediate **6** is 5.2 kcal mol^{-1}. The optimized structures for TS3 and TS4 in the triplet state show imaginary frequency modes at 654 and 257 cm^{-1}, respectively.

Details of electronic structure and spin distribution

Charge densities and spin distributions for compound **1** to **7** and TSs are presented in Table 5. Iron verdoheme with imidazole axial ligand, **1**, is in the triplet ground state with two unpaired electrons on the d orbitals of iron (II). A ferrous verdoheme- O_2 complex, **2**, is formed by pairing one electron of π* orbital of O_2 to one of the πxy or πxz of

Table 5 Calculated Mulliken charges and spin densities for the Fe, **O1** and **O2** atoms, the Imidazole (Im), and the ring macrocycle (values in parentheses are charge densities), the values in bold are NBO charge densities

Compounds	Fe	O1	O2	Ring	Im
1 [a]	1.97	——	——	0.03	0.00
	(1.20)			(−0.34)	(0.14)
	1.25			**−0.34**	**0.09**
2 [a]	1.03	0.27	0.74	0.04	0.00
	(1.52)	(−0.28)	(−0.095)	(−0.32)	(0.18)
	1.48	**−0.29**	**0.06**	**−0.30**	**0.18**
3 [b]	1.08	−0.29	−0.71	0.92	0.00
	(1.50)	(−0.28)	(−0.17)	(−1.24)	(0.14)
	1.55	**−0.34**	**−0.19**	**−1.16**	**0.15**
TS1 [b]	1.05	−0.44	−0.40	0.79	0.00
	(1.55)	(−0.22)	(−0.20)	(−1.30)	(0.17)
	1.51	**−0.35**	**−0.30**	**−1.01**	**0.15**
4 [b]	0.99	0.09	−0.02	−0.06	0.00
	(1.59)	(−0.32)	(−0.27)	(−1.14)	(0.14)
	1.50	**−0.41**	**−0.35**	**−0.85**	**0.11**
TS2 [b]	1.28	−0.32	0.12	−0.08	0.00
	(1.59)	(−0.32)	(−0.33)	(−1.08)	(0.14)
	1.54	**−0.40**	**−0.42**	**−0.86**	**0.14**
5 [c]	1.33	0.87	——	0.80	0.00
	(1.50)	(−0.38)	(−0.46)	(−0.80)	(0.13)
	1.54	**−0.48**	**−0.53**	**−0.64**	**0.11**
TS3 [a]	1.20	0.42	0.41	−0.03	0.00
	(1.63)	(−0.22)	(−0.10)	(−0.50)	(0.19)
	1.59	**−0.29**	**−0.20**	**−0.30**	**0.20**
6 [a]	1.56	0.11	0.014	0.32	0.00
	(1.74)	(−0.28)	(−0.22)	(−0.43)	(0.19)
	1.49	**−0.39**	**−0.30**	**0.00**	**0.22**
TS4 [a]	1.56	−0.35	−0.10	0.80	0.00
	(1.64)	(−0.34)	(−0.31)	(0.17)	(0.18)
	1.54	**−0.36**	**−0.39**	**0.03**	**0.15**
7 [a]	1.40	0.91	——	−0.31	0.00
	(1.56)	(−0.36)	(−0.43)	(0.05)	(0.18)
	1.52	**−0.45**	**−0.49**	**0.13**	**0.29**

[a] Triplet state, [b] Doublet state, [c] Quartet state

the iron. Therefore due to the electronegativity of the oxygen relative to the iron, this electron transfers mainly on the oxygen and the charge on the iron increases from 1.20 in **1** to 1.50 in **2**. Compound **2** is better viewed as iron (III) with an unpaired electron on the iron and the other unpaired electron on the terminal oxygen, Table 5. The terminal oxygen (O_2) has−0.3 charge density while the other oxygen (O1) is almost neutral. So, iron superoxide is a reasonable description of **2**. Compound **3** is formed by the addition of one electron to compound **2**. Table 5 shows that in compound **3** one unpaired electron is placed on the iron and the other unpaired electron is on the macrocycle with parallel spin to the iron ready for bond formation with spin pairing of oxygen and macrocycle (spin density on the iron 1.08 and spin density on the macrocycle 0.92). The terminal oxygen has one unpaired electron (spin density−0.71) with *anti* parallel spin to the other unpaired electron leaving the system three radical with doublet spin state. To further confirm the electronic structures, we performed NBO analysis for compound **3**. Table 6 shows the results of the NBO analysis. This data reveals that the occupancy number of *alpha* and *beta* spin orbital for iron is respectively 2.91 and 1.92; resulting in the net *alpha* spin of 0.98 on the iron. In addition, *alpha* spin orbital for O_2 is 1.96 and *beta* spin orbital for O_2 is 2.90; resulting in the net *beta* spin of 0.99 on the O_2. However one unpaired electron with *alpha* orientation is also present on the ring to make the whole system a doublet.

Spin contamination was assessed and $\langle S^2 \rangle$ value of 1.79 was obtained for compound **3**. This value shows considerable spin contamination and is confirmatory of two unpaired electrons in the σ-FeO_2 and π*-FeO_2 orbitals that are considered as the dz^2 and dyz iron orbitals, respectively (Fig. 5), or a contribution to an admixture of high-spin states. Compound **3** in doublet state, after spin corrected energies (pure doublet), has been stabilized by about 2 kcal mol^{-1}, which showed the increasing of the doublet-quartet splitting (Fig. 3). Figure 5 shows kohn-sham orbitals for the last 6 HOMOs of compound **3**. Based on this figure unpaired electrons are placed on the dz^2 and dyz and a2u like orbital of the macrocycle. Therefore the ring in compound **3** has anion radical nature, since the charge density on the ring is −1.24 and spin distribution is 0.92. Radical nature of macrocycle in **3** makes it vulnerable to a nucleophilic attack by terminal oxygen relative to the intermediate **2**.

Homolysis of oxygen-oxygen bond

In cytochrom p-450 and peroxidase oxygen-oxygen bond is cleaved heterolytically leaving O^+ on the iron and leaving H_2O. Interestingly TS2 in Fig. 6 shows that the charge distribution in two oxygens in transition states are similar (−0.32). This indicates that O-O cleavage is homolytic here and this may be a key feature in verdoheme cleavage in comparison with oxygenase enzyme where a highly reactive intermediate known as compound 1 is formed. Homolytic cleavage in heme catabolism avoids the formation of high reactive species that can initiate oxidative processes. Another argument for homolysis of O-O in intermediate **4** is drawn from details of spin contamination in **4** and **5**. The intermediate **4** in the doublet state has $\langle S^2 \rangle$=0.78 which is in accord with one unpaired electron (spin density on the iron is 0.99) and therefore its spin contamination is negligible. Large value of spin contamination resulted in compound **5** implies the tri-radical nature of this compound

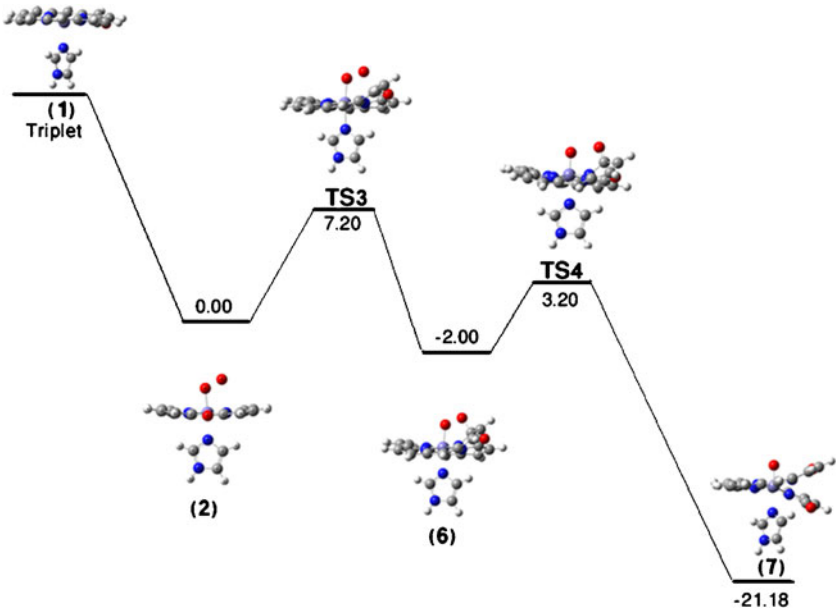

Fig. 4 Computed energy diagram with optimized structures for the reaction species of conversion **2** to **7**

and is yet another indication of hemolytic cleavage of O-O in intermediate **4** [25]. Another important finding in this study arises from detailed electronic analysis of compound **5**. Regarding the literature proposed mechanism for conversion of **2** or **3** to iron biliverdin, the authors believe that iron in high oxidation state similar to compound 1 in oxygenated enzymes is formed [9, 51]. Thus consecutive reduction is proposed to produce iron (III) biliverdin. There is no evidence here for the formation of this highly reactive high oxidation species in biliverdin. Electronic and charge densities in compound **5** shows that the oxidation state of iron is not changed by oxidative ring opening. Charge density on the iron going from **2** to **5** remains fixed around 1.5 consistent with the formation of iron (III) oxidation state. It seems that after homolysis takes place, the electron flow from the ring compensates electron deficiency on the iron. The biliverdin is known as an oxidative distress agent possibly by the same mechanism.

Calculated charges show that in compound **5**, charges on the macrocycle and iron are−0.80 and 1.50 respectively, while for those in compound **7**, charges on the macrocycle and iron are 0.05 and 1.56 respectively. It shows that the added electron in compound **5** is more localized on the ring and does not affect the charge on the iron and thus oxidation state of iron remains 3 in **5** and **7** compounds.

Data of Fig. 7 suggest that compound **5** is a tri-radical species with three unpaired electrons. Table 5 shows that in compound **5** one unpaired electron is placed on the iron, and the other unpaired electron is on the oxygen with parallel spin (spin densities on the iron and on the oxygen are 1.33 and 0.87, respectively). The Fe=O moiety of this species is a triplet state, much like the ground state of dioxygen molecule. The macrocycle has one unpaired electron (spin density 0.80) with parallel spin to the other unpaired electron in the quartet state (former electron is of *anti* parallel spin to the other unpaired electron in the doublet state case). Latos-Grazynnski et al. and Ghosh et al. have shown the radical character of iron biliverdin [52, 53]. The three electrons are, in turn, coupled into two closely low lying spin states: Based on DFT calculations using the B3LYP functional and a variety of basis sets, the ground state of compound **5** is a quartet spin state which is labeled in Fig. 7 and which possesses three unpaired electrons in the π* and LUMO of ring that are coupled ferro magnetically $^4\Psi$ or *anti*-ferro magnetically to generate a doublet spin.

Table 6 NBO analysis of electron distribution **a)** in iron and **b)** in O_2 atoms in compound **3**

Alpha spin orbital		Beta spin orbital	
Occupancy	Orbital	Occupancy	Orbital
a)			
0.98020	LP (1)Fe	−0.97635	LP (1)Fe
0.96952	LP (2)Fe	−0.94835	LP (2)Fe
0.96267	LP (3)Fe	-	-
Sum of alpha spin electron		Sum of beta spin electron	
2.9124		−1.9247	
b)			
0.99802	LP (1)O_2	−0.99851	LP (1)O_2
0.96411	LP (2)O_2	−0.98218	LP (2)O_2
-	-	−0.98020	LP (3)O_2
Sum of alpha spin electron		Sum of beta spin electron	
1.9621		−2.9609	

LP lone pair

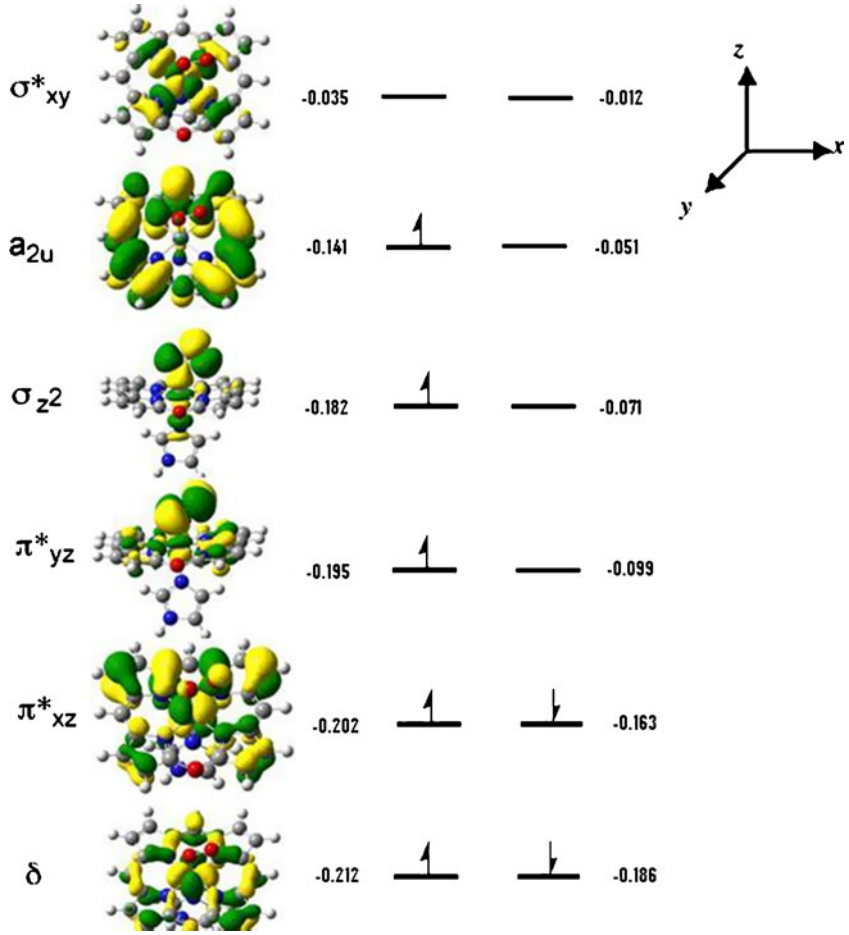

Fig. 5 Kohn-Sham orbitals for the last 6 HOMOs of compound **3**

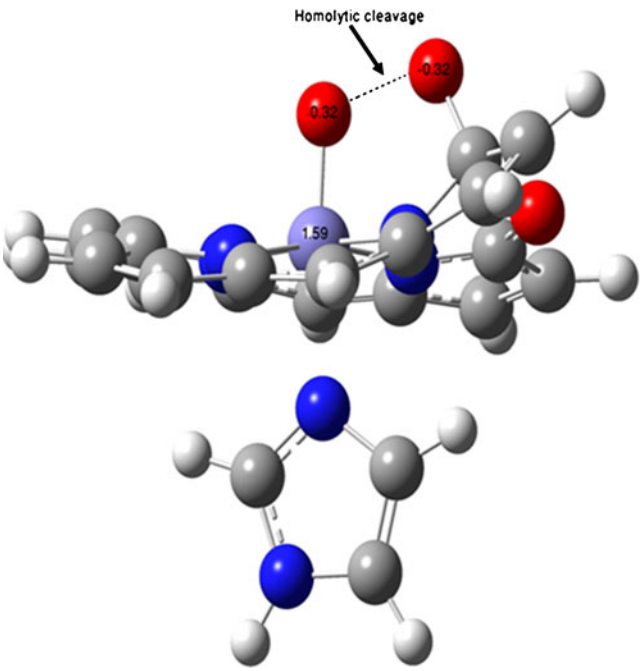

Fig. 6 Optimized structure of TS2 with charge distribution in two oxygen and iron atoms

Figure 8 shows SOMOs (singly occupied molecular orbitals) for compound **5**. As it is evident two unpaired electrons are placed in dxy and dxz iron orbitals. The third unpaired electron is on the LUMO of the biliverdin ligand. This a2u like orbital is stabilized relative to that of a2u orbital of porphyrins due to higher electronegativity of oxygens relative to the carbon.

Spin contamination of the doublet state is assessed and $\langle S^2 \rangle$ value of 1.85 has been obtained. This value shows considerable spin contamination and is confirma-

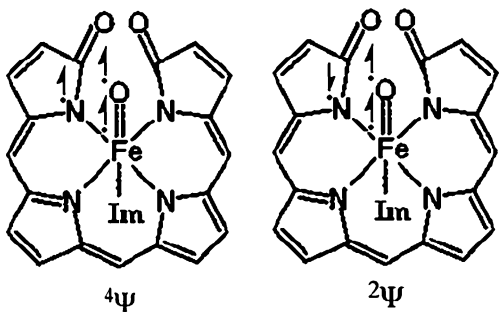

Fig. 7 Two cartoons representing different electronic aspects of the compounds **5**

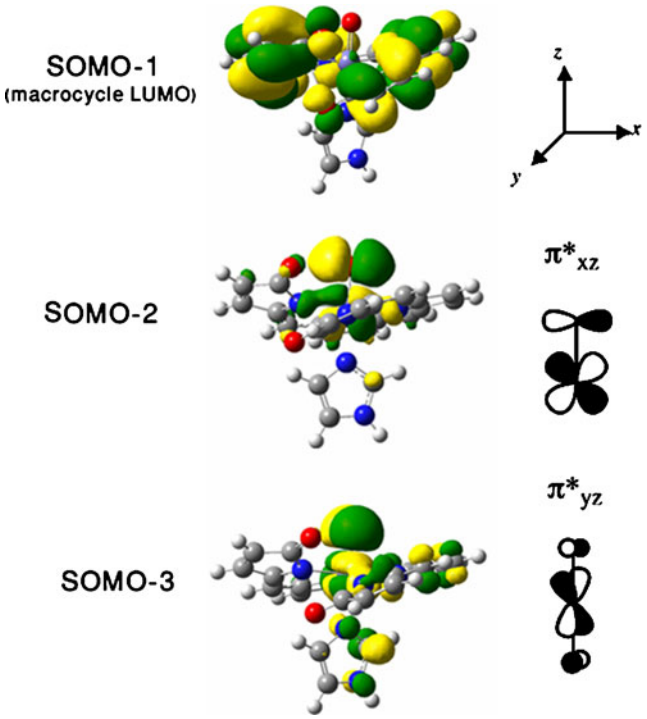

Fig. 8 Kohn-Sham orbitals for the last 3 SOMOs of compound **5**

tory of two unpaired electrons in the π*-FeO orbitals that are considered as the dxy and dxz iron orbitals (Fig. 8), or a contribution to an admixture of quartet states. The compound **5** in doublet state after spin corrected energies (pure doublet), has been destabilized by 1.63 kcal mol^{-1}, which showed the increasing of the doublet-quartet splitting.

Protonation of ferric peroxide intermediate and its effect on the energy surfaces

In this path conversion of ferric hydro peroxide, **8**, to closed ring iron biliverdin, **9**, has a barrier energy of 21 kcal mol^{-1} which is 12.3 kcal mol^{-1} higher than the ferric peroxide path, see Fig. 9. In addition the barrier energy from **9** to **10** (keto-enol) is 9.5 kcal mol^{-1} which is 6 kcal mol^{-1} higher than that for **4** to **5**. The ring opening process from compound **9** to **10** is endothermic with Δ E= 3.77 kcal mol^{-1}.

In conclusion, protonation of oxygen causes a high energy barrier in rate determining step and results in a very slow conversion of ferric hydro peroxide intermediate to biliverdin. Thus protonation could not be involved in the verdoheme breakage to biliverdin.

Non-specific solvent effect

Non-specific solvent effects using the self-consistent reaction field method (SCRF) [54] on the gas phase optimized structures has been considered. Dielectric constant of 80 (ε_0 for water is 78.5) has been chosen to account for the highest non-specific solvent effect.

Considering the effect shown in Fig. 3, the overall change lies in the range of 0.5 to 2 kcal mol^{-1}. The most notable change in this case is observed for **TS1** in the quartet state which has been destabilized by about 5 kcal mol^{-1} and compound **5** in the doublet state which has been stabilized by about 7 kcal mol^{-1}. However, the product in doublet state has been found to become

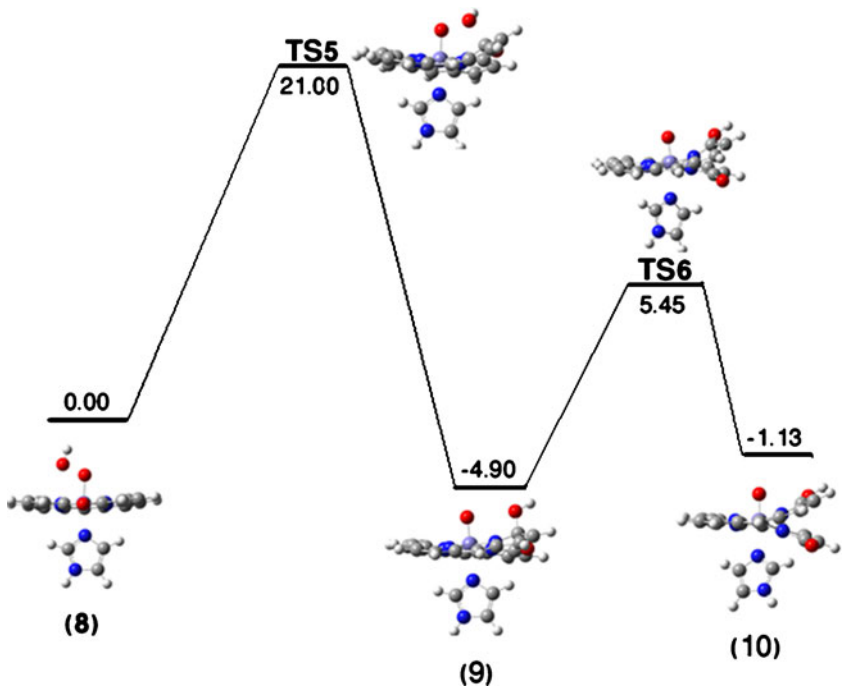

Fig. 9 Computed energy diagram with optimized structures for the reaction species of conversion process of iron verdoheme to iron biliverdin in the presence of H^+

stabilized by about 3 kcal mol^{-1}. Although, such stabilization and destabilization have been caused by an exaggerated solvent effect relative to the natural protein case, the net effect is consistent with the result obtained in the gas phase. Thus, it turns out that the non-specific solvent effect in its extreme case does not alter the gas phase results, in particular if we consider the milder natural condition of protein as the actual solvent. Therefore, for these situations the effect of hydration is negligible. After all, although the solvent effect can be of considerable amount for small charged species, its apparent effect for uncharged macromolecules is small. However the real effect of the physiological condition remains as a scientific challenge. The relative stabilization energies for compounds **3–5** and involved transition states using non-specific solvent effect are presented in the supplementary material.

Conclusions

The ring opening process of ferrous verdoheme to ferric biliverdin was studied in the presence of oxygen, electrons and protons. Energy surfaces have shown that direct attack of O_2 to ferrous verdoheme followed by reduction by one electron to form ferric peroxide verdoheme, **3**, is a most favorable path. In this path oxidation products followed by one electron reduction is exothermic by 32.7 kcal mol^{-1} energy while elimination of reduction by one electron produces 21.8 kcal mol^{-1} energy. In both paths concerted homolytic O-O cleavage and O transfer to the 5-oxo position has low barrier energy in contrast with hydroxylation at the *meso* position of heme by O_2 in the early state of heme catabolism. Protonation of ferric peroxide to form ferric hydroperoxid reduces the rate of oxygenation considerably and cannot be considered as a physiological path. Details of the electronic nature of the intermediates in this process is discussed and some light has been shed on the mechanism of conversion of verdoheme to biliverdin, the least known process in the heme degradation process.

Acknowledgments We are grateful to Prof. Seik Weng Ng for making his software and hardware (machine time) facilities available to us. We thank Dr. Homayoon Bahrahim for useful discussion and the Research Council of Shahid Beheshti University for financial support.

References

1. Liv Y, Moenne-Loccoz P, Loehr TM, Ortiz de Montellano PR (1997) J Biol Chem 272:6909–6917
2. Yoshida T, Noguchi M, Kikuchi G (1980) J Biol Chem 255:4418–4420
3. Ortiz de Montellano PR, Auclair K (2003) In: Kadish KM, Smith KM, Guilard R (eds) The porphyrin handbook. Heme oxygenase structure and function. Elsevier, New York 12, pp 183–210
4. Johnson JA, Olmstead MM, Stolzenberg AM, Balch AL (2001) Inorg Chem 40:5585–5595
5. Koerner R, Latos-Grazynski L, Balch AL (1998) J Am Chem Soc 120:9246–9255
6. Rivera M, Zeng Y (2005) J Inorg Biochem 99:337–354
7. Yoshida T, Migita CT (2000) J Inorg Biochem 82:33–41
8. Balch AL, Koerner R, Olmstead MM, Safari N, Claire ST (1995) J Chem Soc Chem Commun 6:643–644
9. Lad L, Friedman J, Li H, Bhaskar B, Ortiz de Montellano PR, Poulos TL (2004) Biochemistry 43:3793–3801
10. Damaso CO, Rubie ND, Moenne-Loccoz P, Rivera M (2004) Inorg Chem 43:8470–8478
11. Sano S, Sano T, Morishima I, Shiro Y, Maeda Y (1986) Proc Natl Acad Sci USA 83:531–535
12. Gheidi M, Safari N, Bahrami H, Zahedi M (2007) J Inorg Biochem 101:385–395
13. Frisch MJ, Trucks GW, Schlegel HB, Scuseria GE, Robb MA, Cheeseman JR, Zakrzewski VG, Montgomery JA, Stratmann RE, Burant JC, Dapprich S, Millam JM, Daniels AD, Kudin KN, Strain MC, Farkas O, Tomasi J, Barone V, Cossi M, Cammi R, Mennucci B, Pomelli C, Adamo C, Clifford S, Ochterski J, Petersson GA, Ayala PY, Cui Q, Morokuma K, Malick DK, Rabuck AD, Raghavachari K, Foresman JB, Cioslowski J, Ortiz JV, Stefanov BB, Liu G, Liashenko A, Piskorz P, Komaromi I, Gomperts R, Martin RL, Fox DJ, Keith T, Al-Laham MA, Peng CY, Nanayakkara A, Ghonzalez CV, Challacombe MW, Gill PM, Johnson BG, Chen W, Wong M, Andres JL, Head-Gordon M, Replogle ES, Pople JA (1998) Gaussian 98, Rev A.9. Gaussian, Inc, Pittsburgh
14. Parr RG, Yang W (1989) Density-function theory of atoms and molecules. Oxford University Press, Oxford
15. Cramer CJ (2002) Essentials of computational chemistry: theories and models. Wiley, Chichester
16. Siegbahn EM (2003) Faraday Discuss 124:289–296
17. Becke A (1993) J Chem Phys 98:5648–5652
18. Ditchfield R, Hehre WJ, Pople JA (1971) J Chem Phys 54:724–728
19. Petersson GA, Al-Laham MA (1991) J Chem Phys 94:6081–6090
20. Lee C, Yang W, Parr RG (1988) Phys Rev B 37:785–789
21. Vosko SH, Wilk L, Nuasair M (1980) J Phys 58:1200–1211
22. Stephens PJ, Devlin FJ, Chabalowski CF (1994) J Phys Chem 98:11623–11627
23. Yoshizawa K, Kamachi T, Shiota Y (2001) J Am Chem Soc 23:9806–9816
24. Shiota Y, Yoshizawa K (2000) J Am Chem Soc 122:12317–12326
25. Wittbrodt JM, Schlegel HB (1996) J Chem Phys 105:6574–6577
26. Groenhof AR, Swart M, Ehlers AW, Lammertsma K (2005) J Phys Chem A 109:3411–3417
27. Reiher M (2002) Inorg Chem 41:6928–6935
28. Swart M (2008) J Chem Theory Comput 4:2057–2066
29. Paulsen H, Duelund L, Winkler H, Toflund H, Trautwein AX (2001) Inorg Chem 40:2201–2203
30. Balch AL, Latos-Grazynski L, Noll BN, Olmstead MM, Szterenberg L, Safari N (1993) J Am Chem Soc 115:1422–1429
31. Ghosh A, Gonzalez E, Vangberg T (1999) J Phys Chem B 103:1363–1367
32. de Visser SP, Ogliaro F, Harris N, Shaik S (2001) J Am Chem Soc 123:3037–3047
33. Harris D, Loew G (1998) J Am Chem Soc 120:8941–8948
34. Ghosh A, Wondimagegn T (2000) J Am Chem Soc 122:8101–8102
35. Green MT (1999) J Am Chem Soc 121:7939–7940
36. Antony J, Grodzicki M, Trautwein AX (1997) J Phys Chem A 101:2692–2701
37. Green MT (1998) J Am Chem Soc 120:10772–10773
38. Green MT (2000) J Am Chem Soc 122:9495–9499
39. Harris D, Loew G, Waskell L (2001) J Inorg Biochem 83:309–318
40. Kamachi T, Yoshizawa K (2003) J Am Chem Soc 125:4652–4661

41. Hata M, Hirano Y, Hoshino T, Tsuda M (2001) J Am Chem Soc 123:6410–6416
42. Kumar D, de Visser SP, Shaik S (2005) J Am Chem Soc 127:8204–8213
43. Meunier B, de Visser SP, Shaik S (2004) Chem Rev 104:3947–3980
44. Kamachi T, Yoshizawa K (2005) J Am Chem Soc 127:10686–10692
45. Sun J, Wilks A, Ortiz de Montellano PR, Loehr TM (1993) Biochemistry 32:14151–14157
46. Sun J, Loehr T, Wilks A, Ortiz de Montellano PR (1994) Biochemistry 33:13734–13740
47. Ito-Maki M, Kazunobu I, Matera KM, Sato M, Ikeda-Saito M, Yoshida T (1995) Arch Biochem Biophys 317:253–258
48. Schuller DJ, Wilks A, Ortiz de Montellano PR, Poulos TL (1999) Nat Struct Biol 6:860–867
49. Schuller DJ, Zhu W, Stojiljkovic I, Wilks A, Poulos AT (2001) Biochemistry 40:11552–11558
50. Springer BA, Sligar SG, Olson JS, Phillips GN Jr (1994) Chem Rev 94:699–714
51. Lad L, Ortiz de Montellano PR, Poulos TL (2004) J Inorg Biochem 98:1686–1695
52. Wasbotten I, Ghosh A (2006) Inorg Chem 45:4914–4921
53. Szterenberg L, Latos-Grazynnski L, Wojaczynski J (2003) ChemPhysChem 4:691–698
54. Wong MW, Frisch MJ, Wiberg KB (1992) J Am Chem Soc 114:1645–1652